The effects of hindered settling on submarine lobe architecture

Utrecht University

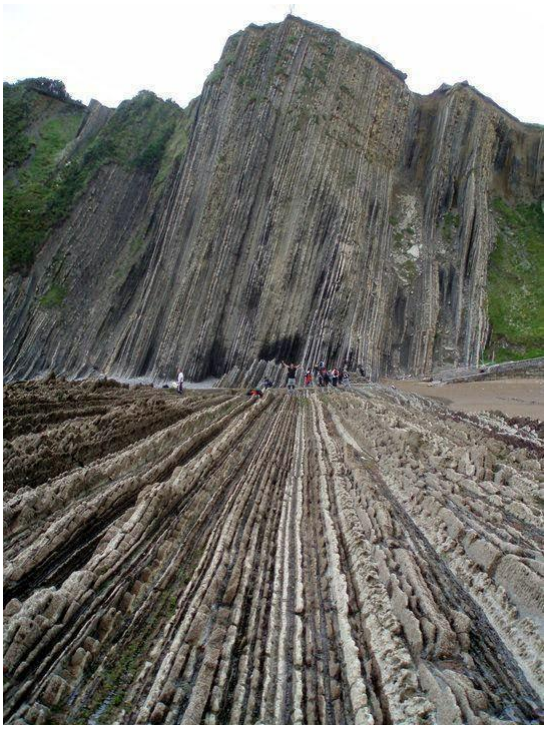

Credit: http://unconventionalgeology.blogspot.com/2012/01/turbidite-sequences.html

Master thesis report
Department of Earth Sciences
Utrecht University

Adam Horst
5648173

Supervisors
Dr. J.T. Eggenhuisen
Dr. J.P. Trabucho Alexandre

Abstract

Submarine lobes form the final stretches of deepmarine sedimentary systems and are important targets for hydrocarbon exploration and production. Therefore, reliable predictions of reservoir geometry are important. However, seismic data sets are typically limited in the amount of detail they can resolve. Furthermore, outcrops of submarine lobes, which could serve as reservoir analogues are often only partially exposed in outcrop.

Model studies can potentially make predictions about parts of the subsurface where information is limited. However, predictive models of lobe deposits are scarce and still at an early stage. In this study, an advection-settling model is presented that accounts for hindered settling. The model allows to make predictions on lobe geometry based on vertical grain size stratification, flow velocity and current duration. With this tool, the influence of hindered settling on lobe geometry has been investigated.

The new model has been tested by modelling flume scale turbidity currents. Results show that incorporation of hindered settling can contribute to more realistic predictions of lobe apex thickness. The lobe thickness maximum is located further basinward for high density currents (>3% vol.), due to the effects of hindered setting. Its effects were found to increase with initial sediment concentration of the parental turbidity current. Moreover, settling velocities of finer grain sizes in turbidity currents are more affected by hindered settling.

To further improve the predictive value of the model, additional processes need to be accounted for. Further work is necessary on incorporation of turbulence production at the break of slope, erosion at the channel-lobe transition zone and flow non-uniformity in turbidity currents.

Keywords: turbidity currents, submarine lobes, hindered settling, predictive modelling, channel-lobe transition zone

Contents

1. Introduction

Terminal lobes form the final stretch of source-to-sink systems in many deepwater environments (figure 1). These deposits are imperfect recorders of climatic, eustatic or tectonic variations at basin margins (Prélat et al., 2010). Moreover, submarine lobes can form good reservoirs for accumulations of hydrocarbons (Mutti et al., 2009).

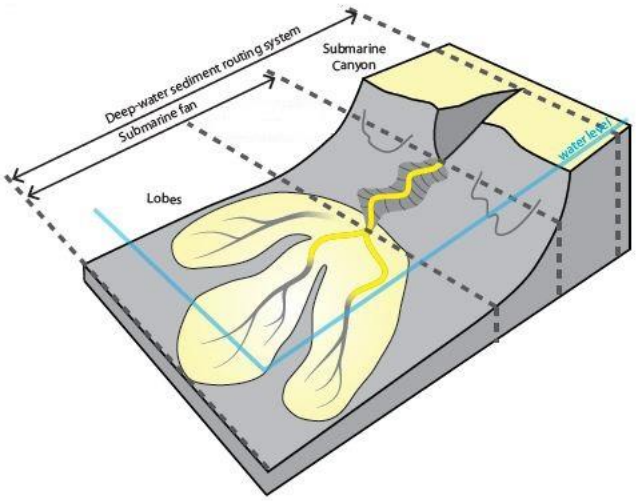

Figure 1: Overview of a deepwater depositional system. After De Leeuw, 2017.

However, studies of reservoir potential of submarine lobes is hampered by limited exposure in outcrop analogues and by the amount of detail that seismic datasets can resolve (Hodgson et al., 2006). Moreover, direct process-product links for submarine lobe environments have mainly been studied by physical experiments (e.g. Spychala et al., 2020; Baas et al., 2004).

Numerical models have the potential to make predictions about parts of the subsurface where information is limited. Additionally, they could provide more insight into process-product links for turbidites. Nevertheless, models that are able to predict lobe architecture from information on the up-dip supply system are scarce.

Spychala et al. (2020) proposed the advection-length method (Ganti et al., 2014) (figure 2) as a tool to estimate lobe element dimensions. The advection-length method describes the transport distance of sediment by means of advection velocity, settling velocity and characteristic grain size of a current. Spychala et al. (2020) tested predictions by this method against the dimensions of their experimental turbidites. They showed that the method is able to predict the first order length dimensions of experimental lobe deposits, as the calculated lengths were around 75% accurate. It was also shown, however, that the lengths of lobe elements were consistently underpredicted.

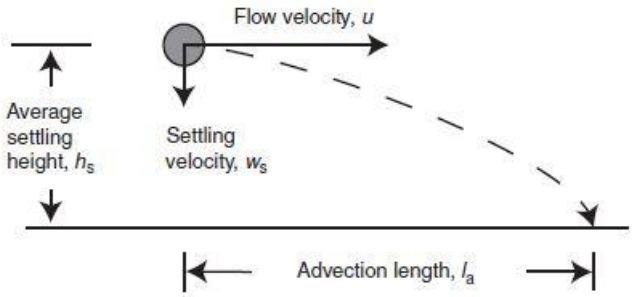

Figure 2: Illustration of the advection-length approach. After Ganti et al., 2014.

Ruliansatri (2020) incorporated the advection-length approach in the EuroSEDS Sediment Budget Estimator (SBE) of Eggenhuisen (under review). The SBE is a simple process model of sediment fluxes through turbidity current channel systems. The purpose of the SBE model is twofold, 1) to bridge the scale gaps between the dynamics of turbidity currents and geological sediment budget estimates and 2) to incorporate modelling into the source-to-sink approach to studying sedimentary systems.

The extension to the SBE made by Ruliansatri (2020) has been called the 'SBE-lobe'. The aim of this extension is to predict the architecture of lobe deposits. In this thesis, the model of Ruliansatri (2020) will be referred to as 'SBE-lobe', whereas the original model developed by Eggenhuisen (under review) will be referred to as 'SBE-channel'. The SBE-lobe is a simplified model that assumes that the break of slope and channel-lobe transition zone (CLTZ) have the same location. It also assumes that turbidity currents transition to a depositional state after exiting the channel system. The model is applicable to a point-source supply system (*sensu* Reading and Richards, 1994) and flat basin floor topography.

The work of Ruliansatri (2020) yielded some interesting results regarding the predicted lobe geometries (figure 3). The model gave a relatively good estimation of lobe thickness in the intermediate and distal areas of the lobe and it could locate the main depocentre of the fine sand grain fraction relatively well. However, some discrepancies were also observed between the model results and architecture known from modern and ancient natural systems. It was shown that the model's largest limitations were in its predictions of lobe apex geometry. SBE-lobe predicted the lobe thickness maximum to be located directly at the lobe apex.

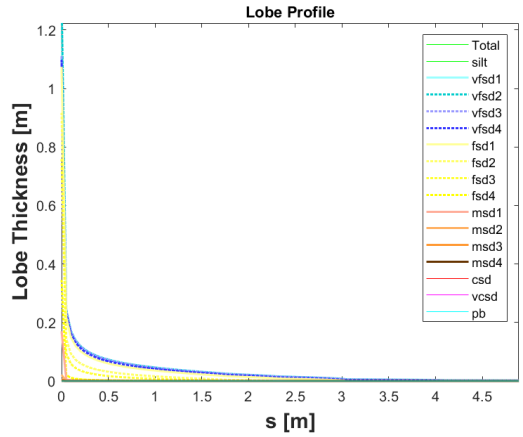

Figure 3: Predicted lobe geometry of SBE-lobe for the boundary conditions of run 5 of De Leeuw et al. (2018). Distance from the lobe apex is on the horizontal axis. After Ruliansatri, 2020.

Datasets from physical experiments (De Leeuw et al., 2018; Spychala et al., 2020) and outcrops (Talling et al., 2007; Wynn et al., 2002) (figure 4) indicate that the lobe thickness maximum of turbidite beds is typically not located directly at the lobe apex. This shows that there is a need for further development of predictive models for lobe deposits.

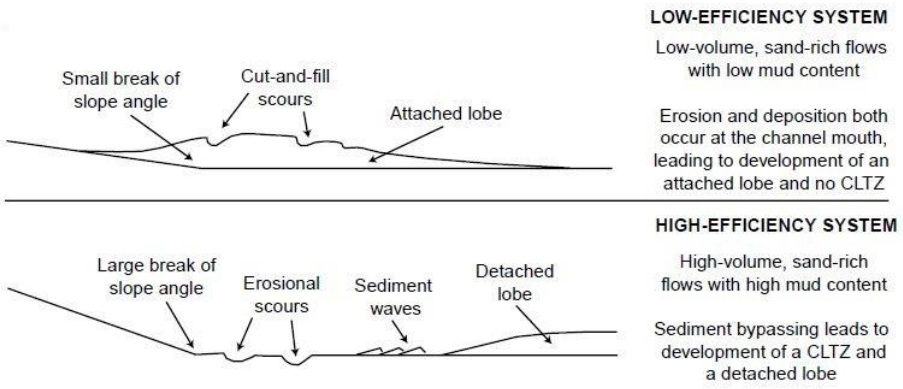

Figure 4: Schematic cross sections through a low-efficiency system with an attached lobe and a high-efficiency system with a detached lobe. After Wynn et al., 2002.

Discrepancies between modelling results and observations from nature and experiment could be related to the dynamic processes that occur at the CLTZ (Pohl, 2019). Spychala et al. (2020) point to the importance of the effects of turbulence and hindered settling. The current study attempts to improve lobe geometry predictions by focusing on the contribution of hindered settling.

Ruliansatri (2020) described sediment settling from turbidity currents with the formulation of Ferguson and Church (2004), which combines Stokes' law and a drag law. However, this formulation is applicable to solitary particles falling through a stationary fluid. At low sediment concentrations, of a few percent (Amy et al., 2006) individual particles can indeed be considered to settle separately. The distance between particles is large enough that they do not interact. It has been observed, however, that the settling velocity of individual particles markedly decreases with other particles in close proximity. This is typically the case when concentrations increase beyond a few percent. This process is referred to as hindered settling (Richardson and Zaki, 1954).

This study focuses on the influence of hindered settling of sediment particles on deposition from turbidity currents. It has been speculated by earlier workers (e.g. Kneller and Branney (1995) and Baas et al. (2004)) that hindered settling can significantly affect deposition from relatively high density turbidity currents.

Hindered settling is a relevant factor to investigate, because turbidity currents tend to have a high degree of sediment stratification (Dorrell et al., 2014), leading to relatively high concentrations towards their bases. Concentrations of more than 10 percent by volume at the base of turbidity currents have been reported by Paull et al. (2018) for natural systems. Moreover, to be able to interpret deposits from turbidity currents, it is important to understand settling of particles at their bases (Dorrell et al., 2011). Furthermore, studying hindered settling can improve our understanding of the processes occurring in small scale turbidity currents in flume laboratories. These flows tend to have relatively high densities due to scaling effects (Pohl et al., 2020). These points emphasize the

importance of studying hindered settling for a better understanding of the processes occurring in turbidity currents.

The aim of this research is to study the influence of hindered settling on submarine lobe architecture. To this end, a simple advection-settling model has been developed, which accounts for hindered settling in its model equations. The new model allows us to test whether incorporation of hindered settling effects contributes to better predictions of submarine lobe architecture.

It is expected that the new model will predict a lower thickness of the lobe apex, compared to models that do not account for hindered settling. The effects of hindered settling are largest in regions of the flow where concentrations are highest (Baas et al., 2004), typically at the base for turbidity currents. Thus, the most proximal deposits, that form by settling from the high concentration regions of the flow, are expected to be most affected by hindered settling processes. In this way, hindered settling could contribute to increased bypass of sediment at the lobe apex.

2. A review of hindered settling literature

To select suitable hindered settling equations for SBE-lobe, a review of literature on this topic has been carried out. Studies focusing on hindered settling typically employ experiments in settling tubes. Such experiments do not account for the effects of turbulence and shear flow, processes which are important for turbidity currents. Nonetheless, these experiments are a useful starting point to grasp the effects of hindered settling at first order.

In the following section the theoretical background of hindered settling will be discussed, which forms the basis of the hindered settling formulations that have been implemented in the SBE-lobe module.

Experiments with uniform suspensions of sediment and fluid have shown that the fall velocity of sediment particles is significantly reduced with respect to that of a single particle, when sediment concentrations are high (Richardson and Zaki, 1954; Van Rijn, 1993). This effect has been argued to be related to several factors. Winterwerp (1999) proposed that the phenomenon of hindered settling is related to three factors, which are viscosity, return currents and buoyancy. Viscosity refers to the drag exerted on settling particles in a viscous fluid. Return currents relate to upward directed flow resulting from continuity effects of particles settling through a fluid. Buoyancy refers to changes in fluid density caused by the presence of sediment.

Richardson and Zaki (1954) have proposed the most often used expression for hindered settling velocity. Their formulation will be referred to as the 'RZ equation'. The equation is based on a power-law correction for the concentration of solids per volume of fluid.

$$w_{s,h} = w_{s,0}(1-\varphi)^n \quad (1)$$

$w_{s,h}$ is hindered settling velocity
$w_{s,0}$ is the fall velocity of a solitary particle
φ is the concentration in volume fraction

$$n = (4.7(1 + 0.15{Re_p}^{0.687}))/(1 + 0.253{Re_p}^{0.687})$$ (Wallis, 1969)

$$Re_p = \frac{w_{s,0} * D * \rho_f}{\mu} \quad (2)$$

D is diameter of the grain

ρ_f is the density of the fluid

μ is kinematic viscosity

The exponent n is higher for smaller particles, which have smaller particle Reynolds numbers. This indicates that the effect of hindered settling is stronger for fine-grained suspensions than for coarse-grained suspensions. The exponent n has been determined experimentally by several workers, the formulation of Wallis (1969) is used in this study.

The variation in the exponent n in the RZ equation accounts for the change in the influence of sediment concentration on particle drag as the Reynolds particle number increases. In this way, the transition between hindered settling in the Stokes and inertial regimes is expressed (Spearman and Manning, 2017).

One of the limitations of the RZ equation is that it does not account for the different behaviour of cohesive and non-cohesive grains. Cohesive particles such as clays have strong electrostatic forces that influence their settling behaviour. In nature, cohesiveness can be enhanced by biogenic molecules that are secreted from diatoms and adhere to particle surfaces (Manning et al., 2011). The discussion and implementation of biogenic flocculation effects is outside the scope of this study, and we will focus on cohesion due to electrostatic forces between clay particles.

Due to these cohesive forces, clay particles in suspension are attracted to one another to form flocs (Spearman and Manning, 2017). When the distance between flocs becomes sufficiently small, they start forming a space filling network. This is known as the gel point (with a volume concentration of φ_{gel}). The gel point marks the transition between hindered settling and the permeability phase of consolidation. During the phase of consolidation, the settling velocity function is mainly driven by the compression of flocs and expulsion of pore water (Spearman and Manning, 2017). The gel concentration is a function of mineralogy, water chemistry and organic content. It typically occurs at clay concentrations between 30 and 180 kg/m^3 (Camenen and Van Bang, 2011), which roughly corresponds to volume fractions between 0.03 and 0.18.

The gel point marks the transition between hindered settling and the permeability phase of consolidation. During this phase, the settling velocity of particles is mainly driven by compression of flocs and expulsion of pore water. After the permeability phase, there is a phase of consolidation where the build-up of stresses within a consolidating bed becomes the dominant process. During this phase, the volume concentration will tend toward the maximum value φ_{max} for cohesive particles (Spearman and Manning, 2017).

The RZ equation does not account for the fact that settling velocity should tend towards zero when suspensions of cohesive particles approach the gelling concentration φ_{gel} or suspensions of non-cohesive particles approach the maximum packing concentration φ_{max} (Spearman and Manning,

2017). φ_{max} is the concentration of non-cohesive particles in the immobile bed underlying a suspension (Baldock et al, 2004).

For these reasons, Spearman and Manning (2017), developed new equations, which rely on the aforementioned empirical parameters. Their equations can be used to model monodisperse suspensions of cohesive or non-cohesive grains at high concentrations.

For cohesive grain size fractions, the following formula is proposed by Spearman and Manning (2017):

$$w_{s,h}^{i} = w_{s,0}^{i}(1-\varphi)(1-\frac{\varphi_{max}}{\varphi_{gel}}\varphi)(1-\frac{\varphi}{\varphi_{gel}})^{1.5} \quad (3)$$

For the non-cohesive grain size fractions, the following formula has been proposed by the same authors:

$$w_{s}^{i} = w_{s,0}^{i}(1-\varphi)^{m}(1-\frac{\varphi}{\varphi_{max}})^{n'} \text{ with } n' = 0.62n - 1.46 \text{ and } m = 2.7 - 0.15n \quad (4)$$

The exponent n' incorporates the effects of sediment volume concentration in the viscosity term and m incorporates the effects of sediment volume concentration in the return current term (Spearman and Manning, 2017). These exponents depend on the earlier discussed exponent n of Richardson and Zaki (1954). For each grain size class in suspension, different exponents n, n' and m have to be calculated.

The unhindered settling velocity $w_{s,0}^{i}$ for both cohesive and non-cohesive sediment was calculated with the equation of Ferguson and Church (2004).

So far, only formulae for hindered settling in monodisperse suspensions have been discussed. Turbidity currents, however, are typically polydisperse suspensions, as indicated by the variety of grain sizes that are found in turbidites (Kane et al., 2017). Equations derived for monodisperse suspensions cannot be directly applied to polydisperse suspensions, because the different grain size fractions interact with each other, leading to different dynamics than predicted by monodisperse formulae (Spearman and Manning, 2017).

For these reasons, more modern formulations have been proposed in literature, the modified MLB (Masliyah (1979), Lockett and Bassoon (1979)) equations, as proposed by Spearman and Manning (2017). The equations are based on a modified version of the Richardson and Zaki (1954) formula. The mMLB equations are also valid for both the Stokes and inertial regimes of particle settling (Spearman and Manning, 2017).

The mMLB approach is based on the following set of equations:

$$W_{s}^{i} = w_{s}^{i} - \sum_{j=1}^{N} \varphi_{j} w_{s}^{j} \quad (5)$$

W_s denotes the settling velocity incorporating all the polydisperse hindered settling effects and w_s is fall velocity in a monodisperse suspension of a specific grain size class (equations 3 and 4) (Spearman and Manning, 2017). The superscripts i refers to the grain size class that settling velocity is modelled for, whereas j refers to the other grain size classes present in suspension. Hindered settling velocities can become negative (i.e. upward directed) in the mMLB formula, especially for the finest grain sizes. Such upward motion of fine particles due to hindered settling effects has also been observed in experiments (Davies, 1968).

3. Model development

Starting point for the modelling efforts of submarine lobe architecture are the vertical grain size stratification of the SBE-channel based on the Rouse equation (Rouse, 1937) and the suspension capacity parameter (Eggenhuisen et al., 2017). The Rouse equation has originally been developed to model suspended sediment concentration in open-channel flow. Eggenhuisen et al. (2020) showed that the equation accurately reproduces the concentration profiles of coarser sediment, but has its limitations in modelling finer particle fractions in subaqueous currents. Despite these notions, the Rouse equation will be applied in this study, in absence of a better empirical formulation for the concentration profile of particles in suspension. The Rouse equation is applied to model concentration profiles for all grain size fractions present in suspension according to the methods of Ruliansatri (2020) and Novianti (2019) (figure 5). To model concentration profiles with the Rouse equation, the grain size distribution at a reference height needs to be known. In the current study, these data are obtained from channel deposit samples.

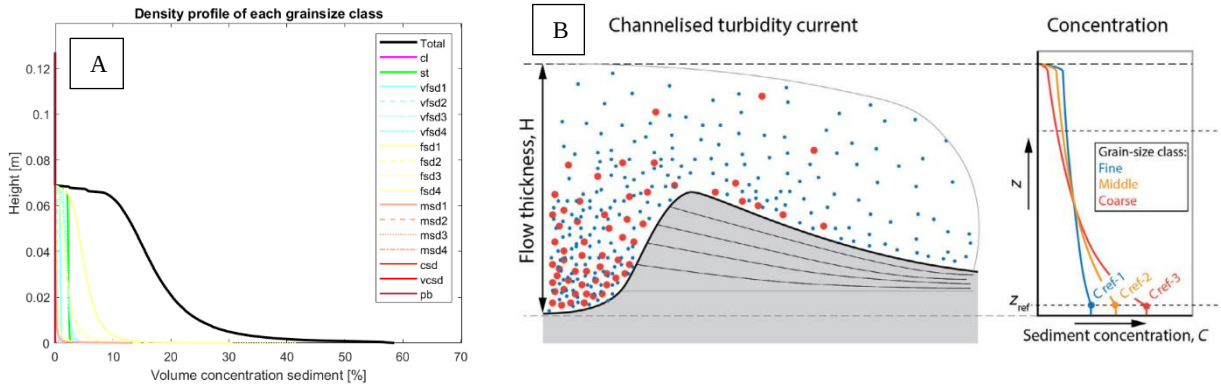

Figure 5: A) Density profiles for the different grain size classes present in suspension. This concentration profile is modelled for the boundary conditions presented in table 1, for a turbidity current with an initial sediment concentration of 19% by vol. B) Conceptual model of grain size stratification in a channelised turbidity current (after Eggenhuisen et al., 2020).

A second boundary condition of the model is mean velocity of channel flow. Mean velocity is based on a one-dimensional velocity profile that is generated by SBE-channel (Eggenhuisen, under review). Spatial evolution of flow velocity in the downstream direction, typically seen in turbidity currents (e.g. Spychala et al., 2020), is not taken into account. Finally, flow duration of the turbidity current in its feeder channel is a necessary boundary condition.

In the developed model, deposition from a turbidity current is assumed to start after it has left the confinement of the channel. Thus, it is assumed that the CLTZ corresponds to a transition from a bypass to a depositional state of the flow and coincides with an abrupt break in slope onto a horizontal basin floor. Deposition continues during the progressive movement of the current over the basin floor.

For each respective grain size class present in suspension, the sediment concentration profile is modelled in SBE-channel. The initial concentration profiles are used in a static manner. The size of the model timestep is based on the time it takes for a specific grain size class to settle over the distance between two adjacent vertical grid points. Thus, at each timestep, a progressively higher cell of the initial concentration profile arrives at the base of the current.

A sediment transport distance increment is calculated by multiplication of the average velocity from the SBE-channel and the timestep size. The sum of all transport distance increments add up to total lobe length for each grain size class.

$$\Delta t = \Delta z / v_s \qquad (6)$$

Δt is timestep size
Δz is grid spacing in the vertical direction
v_s is settling velocity according to the equation of Ferguson and Church (2004)

$$\Delta s = u \times \Delta t \qquad (7)$$

Δs is a transport distance increment
u is average velocity from SBE-channel

In the discussed model approach, turbulence that keeps sediment in suspension is not accounted for after the current has left its channel. Processes of ambient fluid entrainment and substrate erosion are not incorporated either. These simplifications will force the modelled current to be depositional in nature.

The previously discussed mMLB model (eq. 5) (Spearman and Manning, 2017) is used to obtain settling fluxes for the grainsize classes present in suspension as a function of the local concentration at the base of the flow, which varies along the basin floor. The mMLB model has a relatively simple, explicit form and is applicable to polydisperse suspensions that contain a range of grain size classes, both cohesive and non-cohesive.

As discussed in section 2, hindered settling velocities can become negative (i.e. upward directed), according to the mMLB model, especially for the finest grain sizes. Here has been accounted for by a simple budgeting approach in this study, which assumes that material that is transported upward will settle to the bed at a later point in time when hindered settling velocities become positive again.

Deposition from the flow is defined by a flux to the bed at the base of a turbidity current (eq. 8). The flux is based on the concentration of the cell that is located at the bottom of the current at a specific

timestep. Hindered settling is incorporated in the depositional flux at the bottom of the flow, but not higher up in the flow (see eq. 6). The flux depends on three variables: concentration at the base of the flow, hindered settling velocity at the base of the flow and flow duration. In this way, lobe thickness can be modelled along the flow trajectory. The depositional thickness of each respective grain size class is calculated separately, based on the individual concentration profiles. The individual elements are subsequently added to obtain a complete lobe profile for all material transported in a turbidity current. Thus, the vertical sequence of sediment layers in the modelled lobe profiles are not representing the actual vertical stratification but rather is an expression of the relative portion of a specific grain size fraction along the basin floor deposit (Ruliansatri, 2020).

$$Th^i(s) = C_b^i \times W_{s,h}^i \times current\ duration \qquad (8)$$

$Th^i(s)$ is lobe thickness of ith grain size class as a function of distance along the basin floor
C_b^i is the concentration at the base of the current for the ith grain size class
$W_{s,h}^i$ is hindered settling velocity of the ith grain size class taking into account the presence of other particles

As discussed in the review of hindered settling literature (section 2), hindered settling velocities modelled with the mMLB equations can become negative (i.e. upward directed), due to high concentrations in the flow. This is especially the case for the finest grain size classes. Here has been accounted for by a simple budgeting approach, which assumes that material that is transported upward will settle to the bed at a later point in time when hindered settling velocities become positive again.

With equation 8, two-dimensional lobe profiles can be modelled (section 4), with the horizontal axis oriented parallel to the flow direction. The model does not account for processes such as radial spreading and flow thinning (Mohrig and Buttles, 2007) after a turbidity current has left channel confinement.

As discussed earlier, the model only accounts for hindered settling at the base of the flow. Here, its effects are expected to be most pronounced, because the concentration profiles modelled with the Rouse equation have upward decreasing concentrations, especially for the coarser grain size fractions.

To study the effects of hindered settling on lobe geometry (section 4), the model structure described above was slightly adjusted to create an unhindered settling model. The hindered settling velocities in eq. 8 were replaced by unhindered settling velocity formulations of Ferguson and Church (2004). Additionally, the discussed budgeting approach for grain sizes that would obtain upward velocities in a hindered settling model was no longer needed.

An important pitfall of the presented hindered settling model has to be discussed here. A model approach that incorporates hindered settling in the flux at the base of the flow (eq. 8), but not in the flow region above it, creates discontinuities between the two settling regimes. Thus, the condition of conservation of mass is not satisfied in the hindered settling model, because hindered settling velocities at the base of the flow are consistently lower than unhindered settling velocities. This

results in lower deposited sediment loads in hindered settling models compared to unhindered settling models with the same boundary conditions.
The discussed limitations of the presented model does not allow us to make comparisons between hindered and unhindered settling models on all characteristics of modelled sedimentary bodies. Direct comparisons of lobe thickness between hindered and unhindered settling models cannot be carried out. However, comparisons of lobe geometry and location of lobe thickness maxima can still be made and yield informative results.

4. Model results

To investigate the effects of hindered settling on deposit geometry, comparisons are made between models that incorporate hindered settling equations and models that employ the Ferguson and Church (2004) equation for particle settling.

The boundary conditions for the models that will be presented are appropriate for flume-scale experiments and are loosely based on experiments of De Leeuw et al. (2018) and Spychala et al. (2020) (table 1). The boundary conditions are necessary to create sediment concentration profiles and a velocity profile of a characteristic turbidity current. The flow duration properties have been set up to model a single turbidity current event. In this section, model results for turbidity currents with six different initial average sediment concentrations are presented.

Table 1: Boundary conditions and flow duration properties for the models presented in this study.

Boundary Conditions	**Values**
Initial average sediment concentration [% vol.]:	19, 17, 15, 13, 3, 1
Slope angle [^{0}]	11
Flow duration [s]	90
Channel width [m]	0.8
Channel depth [m]	0.05
Bank angles [^{0}]	15; 15
D50; D90	133 µm; 223 µm
Flow duration properties	**Value**
Turbidity current duration [hrs]	0.025
Frequency of turbidity currents [number/year]	1
Geological system activity [kyr]	0.001

As discussed before, grain size distribution data at a reference height are necessary to model concentration profiles with the Rouse equation. In this study, the base of the channel is taken to be the reference height. Grain size distribution data are based on channel deposit samples of run 5 in the physical experiments of De Leeuw et al. (2018). The grain size bins that were created by Ruliansatri (2020) are also used in this study (table 2).

Table 2: Overview of the grain size classes used in the model runs. The frequency and the percentage of the respective grain size classes are from a channel deposit sample taken in run 5 of De Leeuw et al. (2018). The grain size groups, such as 'vf sand', have each been separated into four grain size classes.

No	Grain size term	edgesMID (Phi)	edgesMID (m)	Frequency	Fraction
1	Clay	8.875	0.00000213	0	0.00000
2		8.625	0.00000253	0	0.00000
3		8.375	0.00000301	0	0.00000
4		8.125	0.00000358	0	0.00000
5	vf silt	7.875	0.00000426	0	0.00000
6		7.625	0.00000507	0	0.00000
7		7.375	0.00000602	0	0.00000
8		7.125	0.00000716	0	0.00000
9	f silt	6.875	0.00000852	0	0.00000
10		6.625	0.00001013	0	0.00000
11		6.375	0.00001205	0	0.00000
12		6.125	0.00001433	0	0.00000
13	m silt	5.875	0.00001704	0	0.00060
14		5.625	0.00002026	0	0.00076
15		5.375	0.00002410	0	0.00187
16		5.125	0.00002866	0	0.00094
17	c silt	4.875	0.00003408	0	0.00184
18		4.625	0.00004053	0	0.00157
19		4.375	0.00004819	0	0.00704
20		4.125	0.00005731	0	0.00548
21	vf sand	3.875	0.00006816	0	0.01080
22		3.625	0.00008105	0	0.00606
23		3.375	0.00009639	0	0.03975
24		3.125	0.00011463	0	0.05226
25	f sand	2.875	0.00013631	0	0.21405
26		2.625	0.00016210	0	0.14912
27		2.375	0.00019278	0	0.29005
28		2.125	0.00022925	0	0.10405
29	m sand	1.875	0.00027263	0	0.09277
30		1.625	0.00032421	0	0.01288
31		1.375	0.00038555	0	0.00713
32		1.125	0.00045850	0	0.00098
33	c sand	0.875	0.00054525	0	0.00000
34		0.625	0.00064842	0	0.00000
35		0.375	0.00077111	0	0.00000
36		0.125	0.00091700	0	0.00000
37	vc sand	-0.125	0.00109051	0	0.00000
38		-0.375	0.00129684	0	0.00000
39		-0.625	0.00154221	0	0.00000
40		-0.875	0.00183401	0	0.00000
41	vf pebble	-1.125	0.00218102	0	0.00000
42		-1.375	0.00259368	0	0.00000
43		-1.625	0.00308442	0	0.00000
44		-1.875	0.00366802	0	0.00000
45	f pebble	-2.125	0.00436203	0	0.00000
46		-2.375	0.00518736	0	0.00000
47		-2.625	0.00616884	0	0.00000
48		-2.875	0.00733603	0	0.00000
49	m pebble	-3.125	0.00872406	0	0.00000
50		-3.375	0.01037472	0	0.00000
51		-3.625	0.01233769	0	0.00000
52		-3.875	0.01467206	0	0.00000
	Total			0	1

Simulation parameters needed to run SBE-channel are as presented in appendix 1 of Ruliansatri (2020).

4.1 Lobe profiles for different initial sediment concentrations

In the following section, comparisons of lobe profiles for hindered and unhindered settling models are presented for varying initial sediment concentrations. The impact of hindered settling on deposit geometry will be analysed. In figures 6 to 9, lobe thickness is displayed as a function of distance along the basin floor. The zero point of the horizontal axis represents the lobe apex.

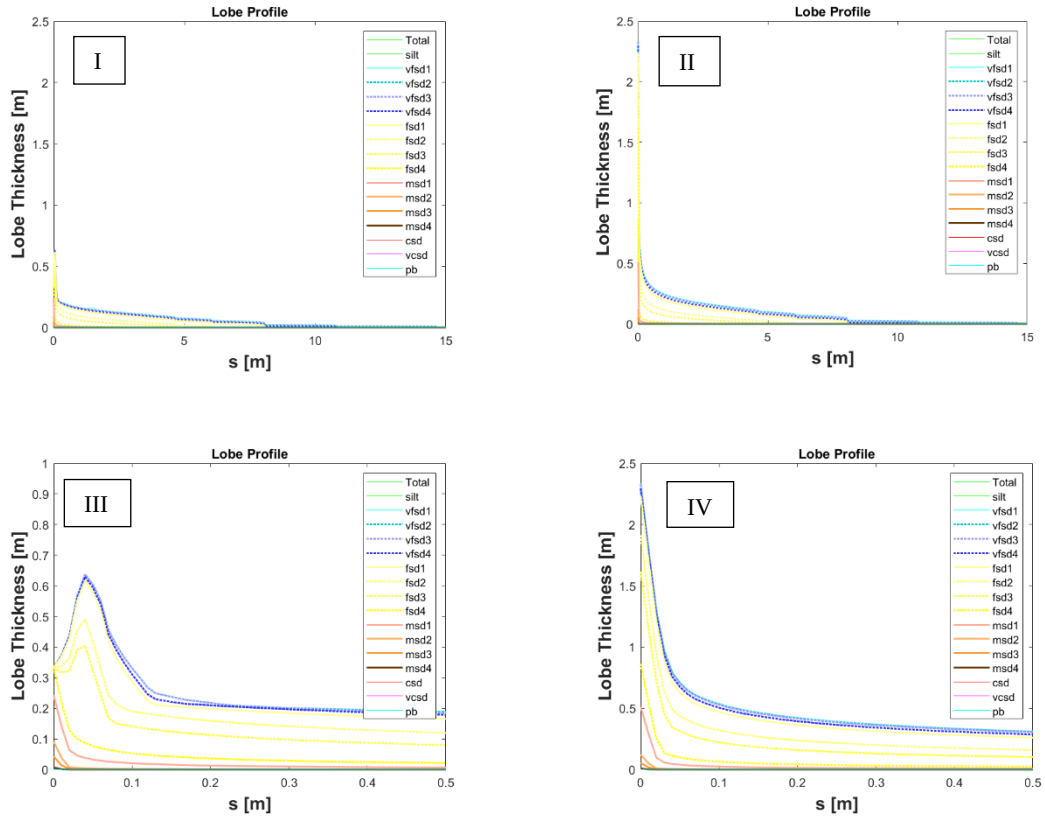

Figure 6: Model predictions for the boundary conditions in table 1. The concentration of the parental turbidity current is 19 % by volume. I) Model with hindered settling II) Model without hindered settling III) Zoom-in of the proximal lobe of the hindered settling model IV) Zoom-in of the proximal lobe of the unhindered settling model

In figure 6, the predicted lobe geometries for a turbidity current with an initial sediment concentration of 19 % vol. are presented. From comparison between figures 6.1 and 6.2, it becomes clear that the application of hindered settling leads to a decrease in lobe apex sedimentation. However, the general concave up shape of the lobe profile is the same for hindered and non-hindered settling models. In figure 6.3 a zoom-in of the proximal lobe geometry for a hindered settling model is provided. It can be seen that the lobe thickness maximum is not located directly at the CLTZ, as is the case for unhindered settling models (figure 6.4).

It is also noted that not all grain size classes are evenly affected by the effects of hindered settling. Grain size classes finer than ‘fine sand 4’ have their thickness maximum at a small distance from the CLTZ. Conversely, grain size classes ‘fine sand 4’ and ‘medium sand’ have their thickness maximum at the CLTZ, the same position as predicted by the non-hindered settling model.

Silt-sized sediment cannot be seen in the figures, because it completely bypasses the lobe deposit. This is due to the fact that silt-sizes sediment obtains an upward velocity along the entire flow trajectory. Thus, it never settles during the presented model runs.

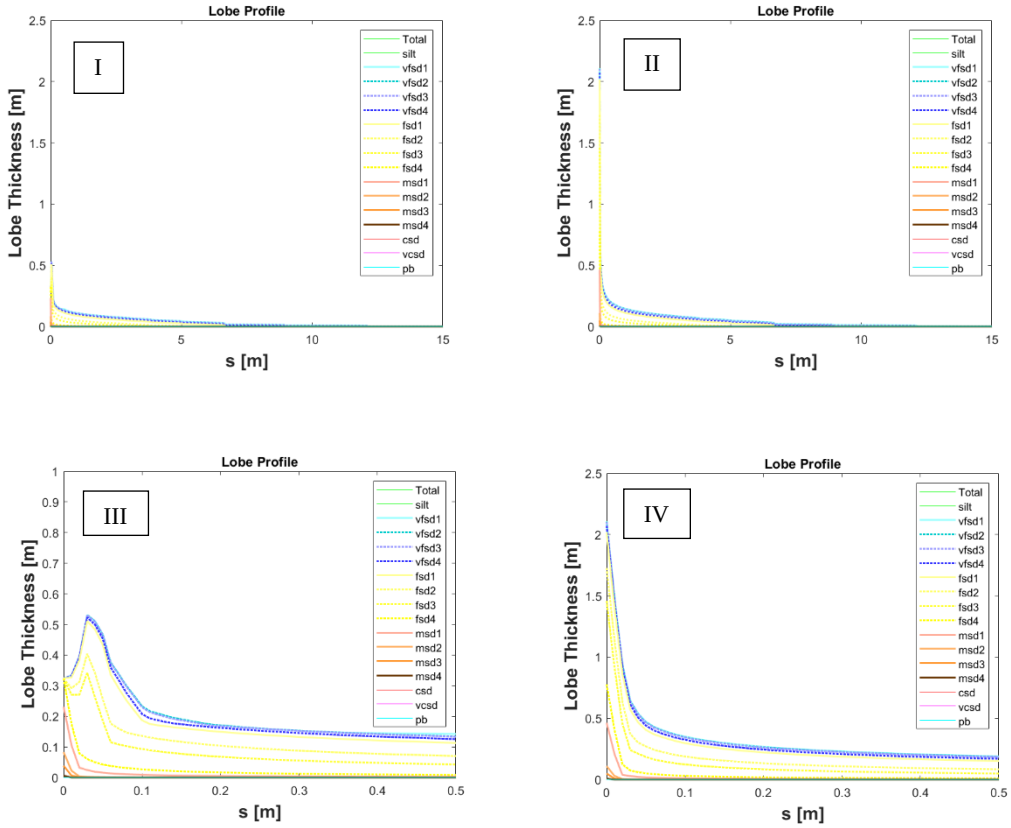

Figure 7: Model predictions for the boundary conditions in table 1. The concentration of the parental turbidity current is 13 % by volume. I) Model with hindered settling II) Model without hindered settling III) Zoom-in of the proximal lobe of the hindered settling model IV) Zoom-in of the proximal lobe of the unhindered settling model

In figure 7, the predicted lobe geometries for a turbidity current with an initial sediment concentration of 13 % vol. are presented. Here, the same observations can be made on the differences between hindered and unhindered settling models as in figure 6. However, because the modelled current has a lower initial sediment concentration, the proximal lobe for both hindered and unhindered settling models is reduced in thickness compared to figure 6.

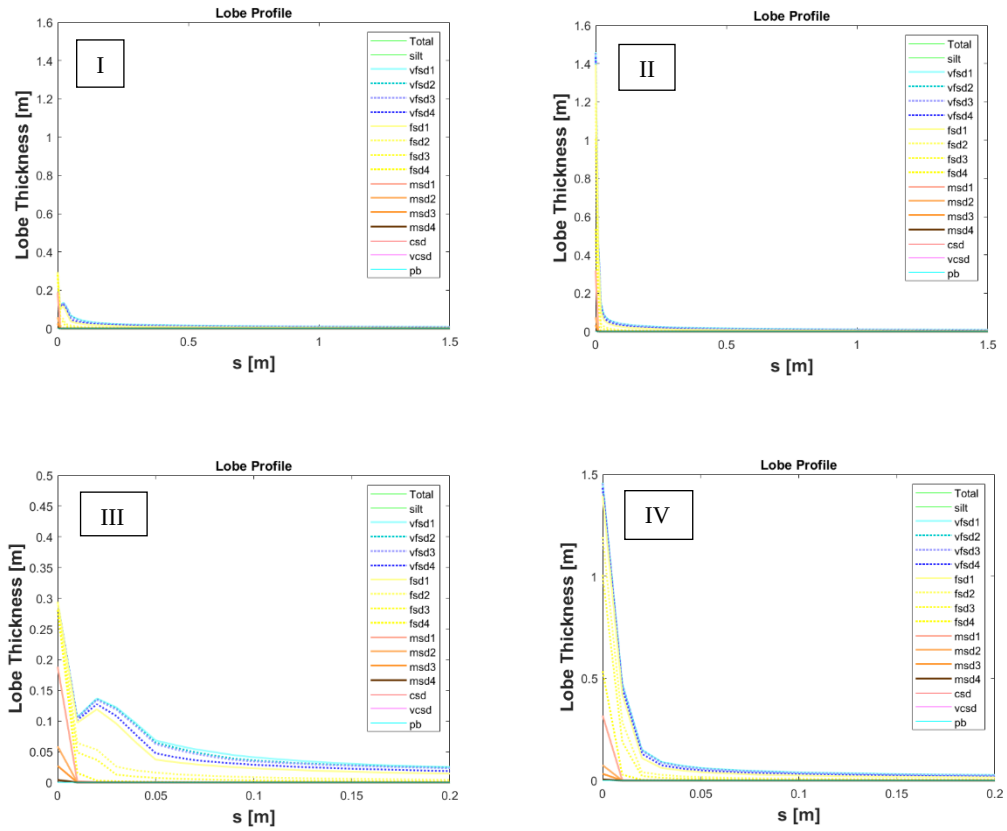

Figure 8: Model predictions for the boundary conditions in table 1. The concentration of the parental turbidity current is 3% by volume. I) Model with hindered settling II) Model without hindered settling III) Zoom-in of the proximal lobe of the hindered settling model IV) Zoom-in of the proximal lobe of the unhindered settling model

In figure 8, the resulting deposit geometry of a current with an initial sediment concentration of 3% is displayed. This time, however, the deposits of both hindered and unhindered settling models have their lobe thickness maximum directly at the lobe apex. Identically to the hindered settling models of figures 6 and 7, the 'fine sand 4' and 'medium sand' grain size classes have their individual thickness maximum at the lobe apex. Conversely, the finer grain size classes have a thickness maximum which is located at a small distance from the lobe apex. Again, lobe apex thickness is significantly reduced for the hindered settling model compared to the unhindered settling model.

In figure 9, the resulting deposit for a current with an initial sediment concentration of 1 % is displayed. Identically to figure 8, the lobe thickness maximum of the hindered settling model is located directly at the lobe apex. However, in this case, only grain size classes 'very fine sand 1' to 'very fine sand 3' have a thickness maximum that is not located directly at the CLTZ. Lobe apex thickness is again significantly reduced when hindered settling is accounted for.

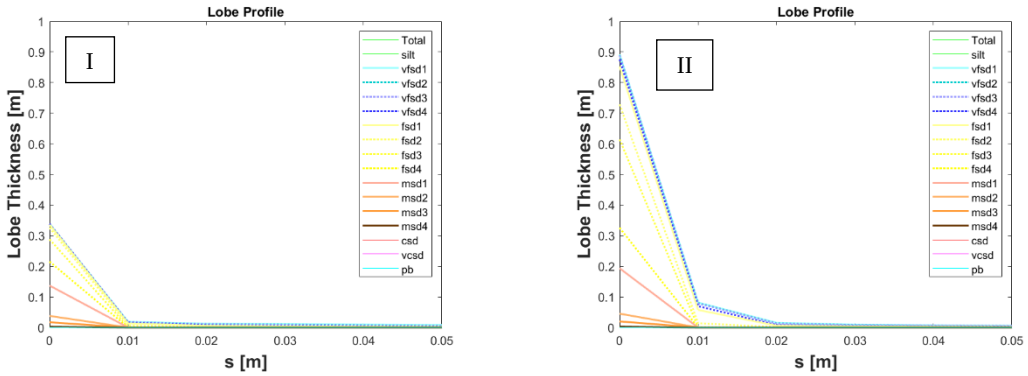

Figure 9: Model predictions for the boundary conditions in table 1. The concentration of the parental turbidity current is 1 % by volume. I) Model with hindered settling II) Model without hindered settling

Figures 6 to 9 indicate that lobe apex thickness in both hindered and unhindered settling models is progressively decreasing with decreasing initial sediment concentration. This can be explained by the relationship between average initial sediment concentration and total carried sediment load of turbidity currents.

In general, the lobe geometries for both hindered and unhindered settling models can be described by a concave up shape. However, for model runs with an average initial sediment concentration higher than 1 % vol., different grain size classes have their thickness maxima at slightly different locations, which creates irregular depositional patterns in the proximal lobes.

From figures 6 to 9, it becomes clear that the effects of hindered settling decrease with decreasing initial sediment concentration of the parental current. Nevertheless, the finest grain size classes discussed (very fine sand) are already affected by hindered settling at relatively low sediment concentrations of 1%.

4.2 Impact of hindered settling on the location of thickness maxima

In figure 10, the location of lobe thickness maxima and thickness maxima of individual grain size groups (silt, very fine sand, fine sand and medium sand) are compared. This has been done for six different initial average sediment concentrations in models that account for hindered settling.

Data for the silt grain size group are not presented, because silt completely bypasses the lobe deposit. The data for the medium sand group are not presented either, because its thickness maximum was located directly at the CLTZ for all concentration runs.

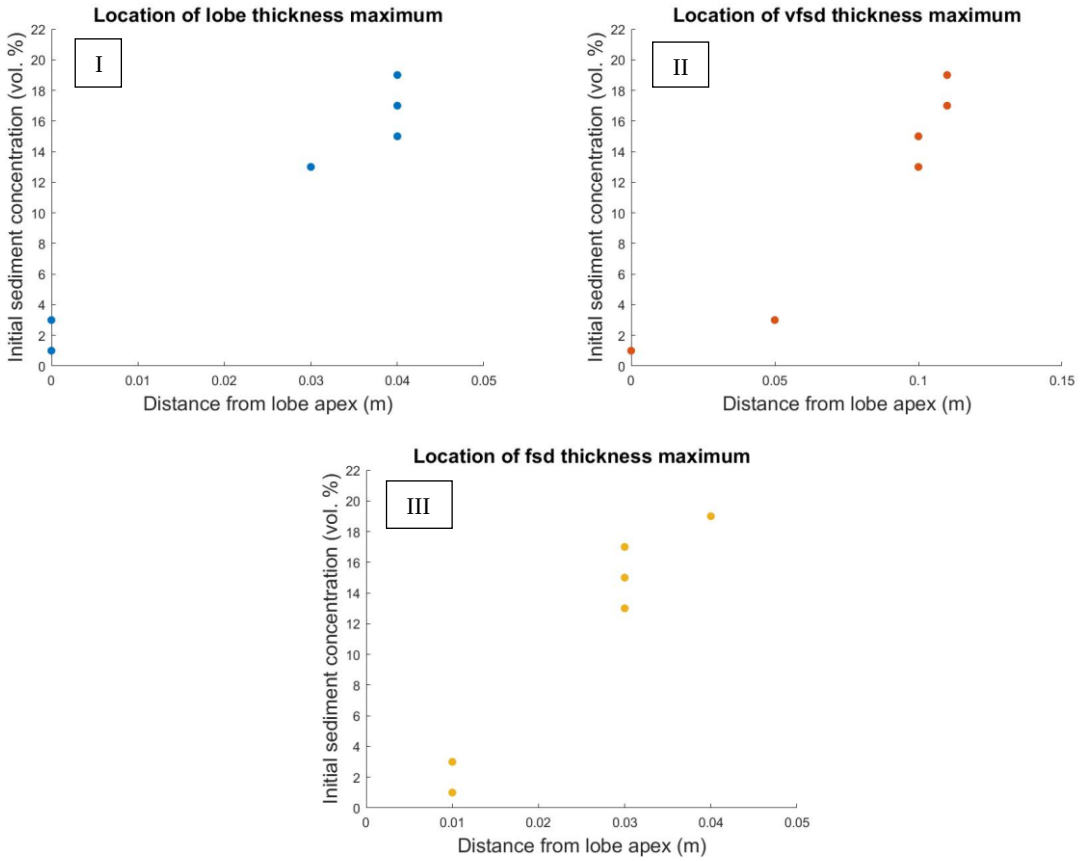

Figure 10: Locations of thickness maxima for hindered settling models with different initial sediment concentrations I) Total lobe thickness maximum II) Thickness maximum of very fine sand III) Thickness maximum of fine sand

The effects of hindered settling are increasing with decreasing grain size. The thickness maximum of the finest grain sizes is located furthest away from the lobe apex. Furthermore, the effects of hindered settling increase with higher initial sediment concentrations of the parental current.

4.3 Comparison of hindered and unhindered settling velocities

In figure 11, hindered and unhindered settling velocities are displayed at the base of a turbidity current with an initial sediment concentration of 19 % vol. It becomes clear that the initial hindered settling velocity when a current leaves the submarine channel is significantly lower than the unhindered settling velocity. Hindered settling velocity increases during the movement of a turbidity current over the basin floor due to the progressive loss of sediment in suspension.

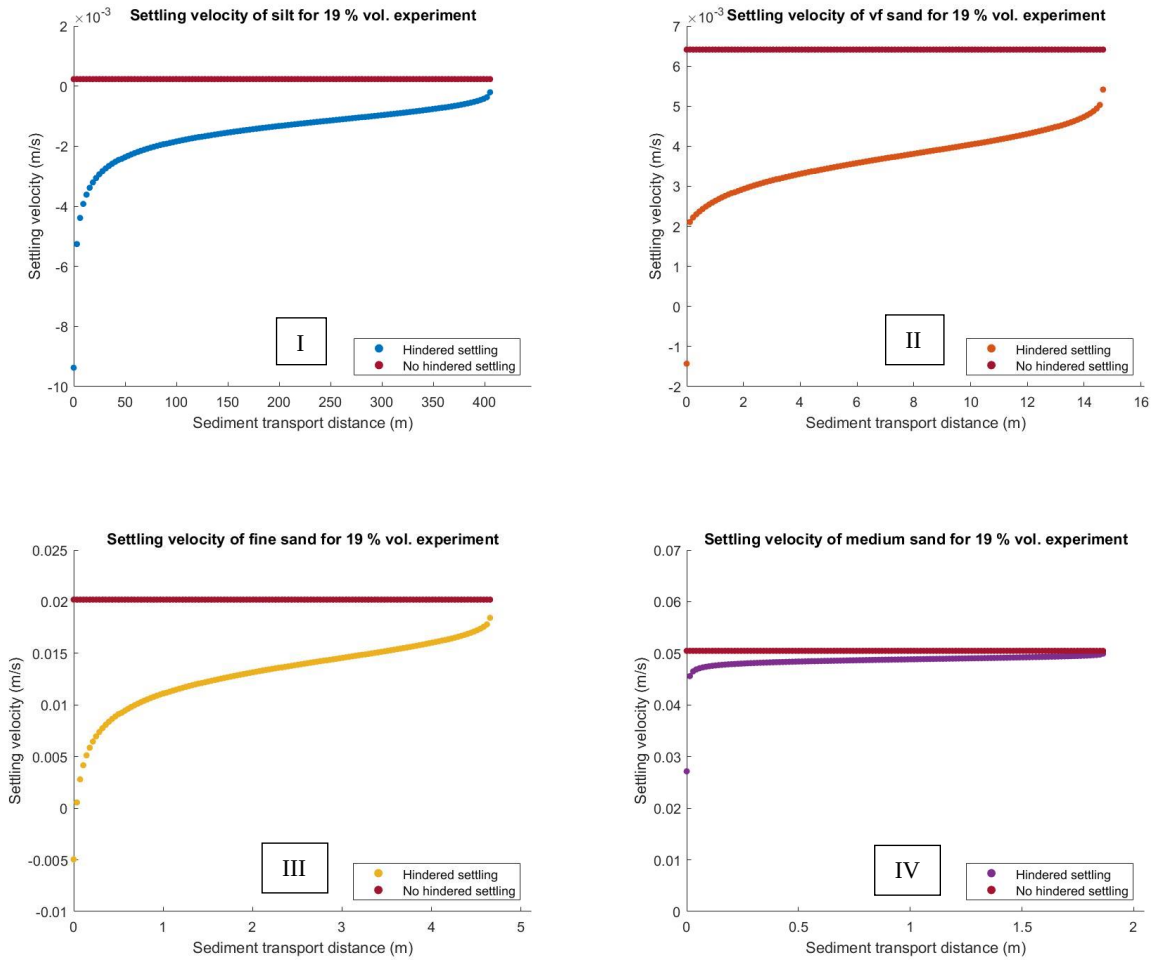

Figure 11: Settling velocity at the base of a turbidity current with an initial sediment concentration of 19 % vol. I) Settling velocities for silt II) Settling velocities for very fine sand III) Settling velocities for fine sand IV) Settling velocities for medium sand

Settling velocities are most reduced at the location of the lobe apex, where the concentration at the base of the current is relatively high. Due to stratification of the current, lower concentrations regions of the flow arrive at the base of the current at localities further away from the lobe apex. In figure 11, it can be seen that the current is affected by hindered settling along its entire trajectory over the basin floor. The hindered settling velocities at the base of the current never equal the unhindered settling velocities.

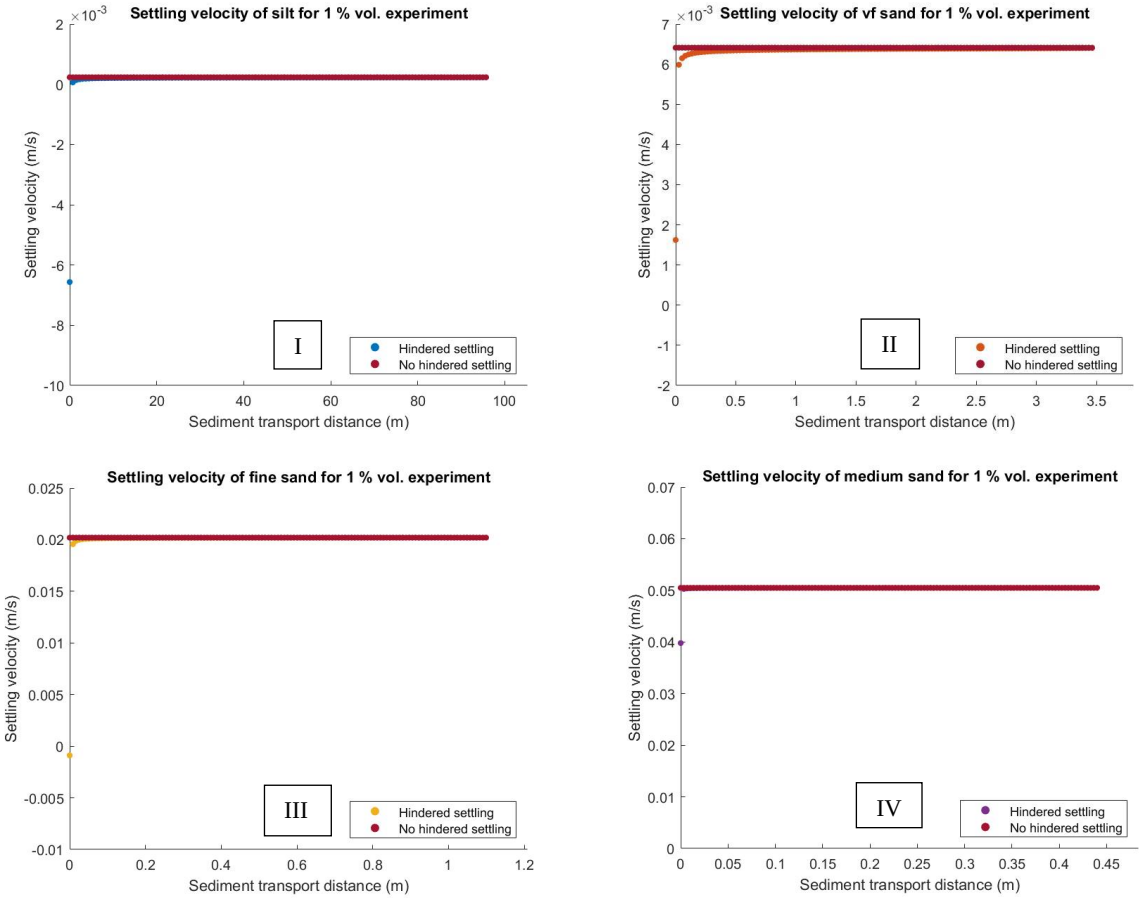

Figure 12: Settling velocities at the base of a turbidity current with an initial sediment concentration of 1 % vol. I) Settling velocities for silt II) Settling velocities for very fine sand III) Settling velocities for fine sand IV) Settling velocities for medium sand

In figure 12, both hindered and unhindered settling velocities are presented at the base of a turbidity current with an initial average sediment concentration of 1 % vol. It can be observed that hindered and unhindered settling velocities are relatively similar. A significant deviation between the two functions only occurs at the lobe apex, where concentrations are relatively high.

Comparisons of figures 11 and 12 show that the intensity of hindered settling is dependent on the initial sediment concentration of the modelled current. In figure 12, the ratio of unhindered to hindered settling velocity is much lower for all grain size groups. In both figures 11 and 12, it is shown that hindered settling velocity is initially much lower at the lobe apex, due to strong stratification of the current. When concentrations at the base of the current decrease at more distal locations on the basin floor, hindered settling velocity progressively increases and approaches the unhindered settling velocity.

5. Discussion

The discussed model results indicate that incorporation of hindered settling in the advection-length method (Ganti et al., 2014; Ruliansatri, 2020) might contribute to more realistic predictions of lobe geometry. The newly developed model showed that hindered settling significantly reduces lobe apex thickness compared to models that employ unhindered settling velocity functions. Moreover, hindered settling can be responsible for basinward shifts in the location of the lobe thickness

maximum in relatively high density (>1 % vol.) currents at the flume scale. This implies that hindered settling can contribute to increased transport of sediment beyond the lobe apex.

It is not surprising that hindered settling has a strong effect on lobe apex sedimentation in the presented models. The highest concentrations of stratified currents arriving at the CLTZ are located at their bases. Material that settles from this high concentration region is most affected by hindered settling. At more distal lobe environments, hindered settling still has an influence on deposition, but its effects are progressively decreasing. Thus, the model results suggest a decreasing effect of hindered settling in a depositional turbidity current along its trajectory over the basin floor.

Remarkably, the hindered settling velocity profiles of figures 9 and 10 show a similar shape to the density profiles shown in figure 3. This observation also suggests that the expression of hindered settling is strongly dependent on the initial sediment stratification of a turbidity current.

The developed model also showed that the effects of hindered settling were most pronounced for relatively fine grain size classes in suspension (silt, very fine sand and fine sand), whereas medium sized sand is relatively unaffected.

To further improve understanding of hindered settling in turbidity currents, additional steps in model development are necessary. The current model only accounts for hindered settling at the base of a turbidity current. Extension of hindered settling to the entire flow depth is expected to increase sediment transport distances, which will also impact lobe geometries.

This hypothesis could be tested by development of a space- and time-resolved numerical hindered settling model. Such a model would be able to create spatially and time resolved concentration fields in a moving turbidity current. This would allow for elucidation of direct feedbacks between concentration and settling velocity in the entire flow.

Realism of the model can also be enhanced by incorporation of other dynamic processes that occur in turbidity currents. Possible model improvements that might contribute to better predictions of lobe characteristics are discussed below.

In the model, a height averaged flow velocity is applied. To obtain more realistic predictions of sediment transport distances, the height-dependency of flow velocity has to be accounted for. Additionally, the model assumes flow uniformity, whereas in physical experiments, turbidity currents have been observed to decelerate after leaving confinement (e.g. Spychala et al., 2020).

Progressive deceleration has a relation with the evolution of turbulence in turbidity currents (Gray et al., 2005). Turbulence is a relevant factor for turbidity current behaviour, because it counteracts particle settling (Eggenhuisen et al., 2020). Changes in turbulent kinetic energy during a current's trajectory over the basin floor are expected to have a strong effect on resulting lobe geometry. Turbulence production might also explain the frequently observed erosional features at the CLTZ (Wynn et al., 2002) and the location of lobe thickness maxima (Spychala et al., 2020). These notions emphasize the importance of considering turbulence effects in studies aiming to model turbidite deposits. Coupling of spatial flow evolution and turbulence evolution could be a large step forward in lobe deposit modelling.

Sediment resuspension processes at the base of the flow can also be important controls on deposit architecture after breaks in slope at CLTZ's (Pohl et al., 2019; Cantero et al., 2012; Talling et al., 2007). Incorporating these processes in the model is necessary to understand the occurrence of erosional features at CLTZ's (Wynn et al., 2002).

6. Conclusions

Hindered settling can contribute to the transport of a larger fraction of a turbidity current's load beyond the lobe apex in turbidity currents at the laboratory scale. In relatively high density flows (>1%) hindered settling also impacts the location of the lobe thickness maximum, which is located at more distal locations for flows with higher initial sediment concentrations. Hindered settling has the strongest effect on the sedimentation of the finest particles in a polydisperse turbidity current.

References

Amy, L. A., Talling, P. J., Edmonds, V. O., Sumner, E. J., & Lesueur, A. (2006). An experimental investigation of sand–mud suspension settling behaviour: implications for bimodal mud contents of submarine flow deposits. *Sedimentology*, *53*(6), 1411-1434.

Baas, J. H., Van Kesteren, W., & Postma, G. (2004). Deposits of depletive high-density turbidity currents: a flume analogue of bed geometry, structure and texture. *Sedimentology*, *51*(5), 1053-1088.

Baldock, T. E., Tomkins, M. R., Nielsen, P., & Hughes, M. G. (2004). Settling velocity of sediments at high concentrations. *Coastal engineering*, *51*(1), 91-100.

Cantero, M. I., Shringarpure, M., & Balachandar, S. (2012). Towards a universal criteria for turbulence suppression in dilute turbidity currents with non-cohesive sediments. *Geophysical Research Letters*, *39*(14).

Davies, R. (1968). The experimental study of the differential settling of particles in suspension at high concentrations. *Powder Technology*, *2*(1), 43-51.

Dorrell, R. M., Darby, S. E., Peakall, J., Sumner, E. J., Parsons, D. R., & Wynn, R. B. (2014). The critical role of stratification in submarine channels: implications for channelization and long runout of flows. *Journal of Geophysical Research: Oceans*, *119*(4), 2620-2641.

Dorrell, R. M., Hogg, A. J., Sumner, E. J., & Talling, P. J. (2011). The structure of the deposit produced by sedimentation of polydisperse suspensions. *Journal of Geophysical Research: Earth Surface*, *116*(F1).

Camenen, B., & van Bang, D. P. (2011). Modelling the settling of suspended sediments for concentrations close to the gelling concentration. *Continental Shelf Research*, *31*(10), S106-S116.

Eggenhuisen, J.T. (under review). The EuroSEDS Sediment Budget Estimator (SBE); integrating a turbidity current process model in Source-to-Sink sediment budget estimates.

Eggenhuisen, J. T., Cartigny, M. J., & de Leeuw, J. (2017). Physical theory for near-bed turbulent particle suspension capacity. *Earth surface dynamics.*, *5*(2), 269-281.

Eggenhuisen, J. T., Tilston, M. C., de Leeuw, J., Pohl, F., & Cartigny, M. J. (2020). Turbulent diffusion modelling of sediment in turbidity currents: An experimental validation of the Rouse approach. *The Depositional Record*, *6*(1), 203-216.

Ferguson, R. I., & Church, M. (2004). A simple universal equation for grain settling velocity. *Journal of sedimentary Research*, *74*(6), 933-937.

Ganti, V., Lamb, M. P., & McElroy, B. (2014). Quantitative bounds on morphodynamics and implications for reading the sedimentary record. *Nature communications*, *5*(1), 1-7.
Gray, T. E., Alexander, J., & Leeder, M. R. (2005). Quantifying velocity and turbulence structure in depositing sustained turbidity currents across breaks in slope. *Sedimentology*, *52*(3), 467-488.
Hodgson, D. M., Flint, S. S., Hodgetts, D., Drinkwater, N. J., Johannessen, E. P., & Luthi, S. M. (2006). Stratigraphic evolution of fine-grained submarine fan systems, Tanqua depocenter, Karoo Basin, South Africa. *Journal of Sedimentary Research*, *76*(1), 20-40.
Kane, I. A., Pontén, A. S., Vangdal, B., Eggenhuisen, J. T., Hodgson, D. M., & Spychala, Y. T. (2017). The stratigraphic record and processes of turbidity current transformation across deep-marine lobes. *Sedimentology*, *64*(5), 1236-1273.
Kneller, B. C., & Branney, M. J. (1995). Sustained high-density turbidity currents and the deposition of thick massive sands. *Sedimentology*, *42*(4), 607-616.
de Leeuw, J. (2017). *The sedimentary record of submarine channel morphodynamics* (Doctoral dissertation, Utrecht University).
de Leeuw, J., Eggenhuisen, J. T., Spychala, Y. T., Heijnen, M. S., Pohl, F., & Cartigny, M. J. (2018). Sediment volume and grain-size partitioning between submarine channel− levee systems and lobes: An experimental study. *Journal of Sedimentary Research*, *88*(7), 777-794.
Lockett, M. J., & Bassoon, K. S. (1979). Sedimentation of binary particle mixtures. *Powder Technology*, *24*(1), 1-7.
Manning, A. J., Baugh, J. V., Soulsby, R. L., Spearman, J. R., & Whitehouse, R. J. S. (2011). *Cohesive sediment flocculation and the application to settling flux modelling* (pp. 91-116). InTech.
Masliyah, J. H. (1979).] Hindered settling in a multi-species particle system. *Chemical Engineering Science*, *34*(9), 1166-1168.
Mohrig, D., & Buttles, J. (2007). Deep turbidity currents in shallow channels. *Geology*, *35*(2), 155-158.
Mutti, E., Bernoulli, D., Lucchi, F. R., & Tinterri, R. (2009). Turbidites and turbidity currents from Alpine 'flysch' to the exploration of continental margins. *Sedimentology*, *56*(1), 267-318.
Novianti, W. (2019). *An Analytical Model to Predict the Sediment Flux of Each Grain-Size Class in Turbidity Current Flow; Application to Gold Channel, Tres Pasos Formation, Chile*. Master thesis Utrecht University.
Paull, C. K., Talling, P. J., Maier, K. L., Parsons, D., Xu, J., Caress, D. W., ... & Chaffey, M. (2018). Powerful turbidity currents driven by dense basal layers. *Nature communications*, *9*(1), 1-9.
Pohl, F. (2019). *Turbidity currents and their deposits in abrupt morphological transition zones* (Doctoral dissertation, UU Dept. of Earth Sciences).
Pohl, F., Eggenhuisen, J. T., Cartigny, M. J. B., Tilston, M. C., de Leeuw, J., & Hermidas, N. (2020). The influence of a slope break on turbidite deposits: an experimental investigation. *Marine Geology*, *424*, 106160.
Pohl, F., Eggenhuisen, J. T., Tilston, M., & Cartigny, M. J. B. (2019). New flow relaxation mechanism explains scour fields at the end of submarine channels. *Nature communications*, *10*(1), 1-8.
Prélat, A., Covault, J. A., Hodgson, D. M., Fildani, A., & Flint, S. S. (2010). Intrinsic controls on the range of volumes, morphologies, and dimensions of submarine lobes. *Sedimentary Geology*, *232*(1-2), 66-76.
Reading, H. G., & Richards, M. (1994). Turbidite systems in deep-water basin margins classified by grain size and feeder system. *AAPG bulletin*, *78*(5), 792-822.
Richardson, J.F., & Zaki, W.N., 1954. Sedimentation and fluidisation: part 1. Trans. Inst. Chem. Eng. 32, 35– 53.

van Rijn, L. C. (1993). *Principles of sediment transport in rivers, estuaries and coastal seas* (Vol. 1006, pp. 11-3). Amsterdam: Aqua publications.

Rouse, H. (1937) Modern conceptions of the mechanics of fluid turbulence. Transactions of the American Society of Civil Engineers, 102, 463–505.

Ruliansatri, V. (2020). *Submarines Lobe Geometry and the Average Grain Size Distribution Prediction based on Its Channel System.* Master thesis Utrecht University.

Spearman, J., & Manning, A. J. (2017). On the hindered settling of sand-mud suspensions. *Ocean Dynamics*, *67*(3-4), 465-483.

Spychala, Y. T., Eggenhuisen, J. T., Tilston, M., & Pohl, F. (2020). The influence of basin setting and turbidity current properties on the dimensions of submarine lobe elements. *Sedimentology*, *67*(7), 3471-3491.

Talling, P. J., Amy, L. A., & Wynn, R. B. (2007). New insight into the evolution of large-volume turbidity currents: comparison of turbidite shape and previous modelling results. *Sedimentology*, *54*(4), 737-769.

Wallis, G. B. (1969). One-dimensional two-phase flow (Vol. 1, pp. 175–281). New York, NY: McGraw-Hill.

Winterwerp, H. (1999). On the dynamics of high-concentrated mud suspensions. *Communications on Hydraulic and Geotechnical Engineering*.

Wynn, R. B., Kenyon, N. H., Masson, D. G., Stow, D. A., & Weaver, P. P. (2002). Characterization and recognition of deep-water channel-lobe transition zones. *AAPG bulletin*, *86*(8), 1441-1462.